



# Winter-to-winter recurrence of the tripole pattern of the sea surface temperature anomalies in the North Atlantic ocean and its interaction with the NAO

Pavel A. Sukhonos<sup>1</sup> · Michael A. Alexander<sup>2</sup>

Received: 12 September 2023 / Accepted: 5 June 2024 / Published online: 14 June 2024  
© The Author(s), under exclusive licence to Springer-Verlag GmbH Germany, part of Springer Nature 2024

## Abstract

The evolution of temperature anomalies in the North Atlantic (15° N – 70° N 80° W – 8° W) is analyzed. The results are based on the decomposition of the GECCO3 (1948–2018), ORA-S5 (1979–2018) and SODA3.12.2 (1980–2017) oceanic reanalyses data using extended empirical orthogonal functions. The leading pattern during the entire 16-month period (January–April of the next year) in the 0–300 m layer is a tripole, with temperature anomalies of the same sign in the tropical and high latitudes and the opposite sign in the subtropical gyre. The evolution of the leading pattern shows the deepening of temperature anomalies in winter, their preservation with a maximum in the summer seasonal thermocline (~65–90 m) and partial weakening in the subsurface layer in summer, and their emergence on the ocean surface in the subsequent autumn–winter season. The temporal evolution of the reemergence of the tripole pattern of the sea surface temperature anomalies (SSTAs), explained by the first extended principal component (EPC1), is in good agreement with the variability of the main atmospheric circulation mode over the North Atlantic on interannual scales – the North Atlantic Oscillation (NAO), especially after 1979. The recurrence of SSTAs is found in all three centers of action of the tripole pattern. In the subpolar and midlatitude centers of action, the reemerging signal maximum appears in the subsurface layer in late summer and early autumn and in the subsequent autumn–winter season ~2/3 of this signal occurs at the surface. In the subtropical center of action, the reemerging signal maximum appears in the mixed layer in winter–spring and in the subsequent autumn–winter season ~1/2 of this signal occurs at the surface. For the subtropical center of action, a moderate correlation was found between the regional EPC1 and the mixed layer depth and the wind stress modulus over a 16-month period. Recurrence of temperature anomalies in all centers of action of the tripole structure from January 2014 to April 2015 associated with the repeated positive NAO phase is shown.

**Keywords** Extended EOF · Granger causality · Reemergence · Tripole · North Atlantic

## 1 Introduction

Temperature anomalies formed at the ocean surface during the winter season propagate downward within the deep winter mixed layer. In the spring–summer period, after a rapid

shallowing of the mixed layer, temperature anomalies can persist in the subsurface layer, isolated from the influence of heat fluxes on the ocean surface by a new thin mixed layer. In the subsequent autumn–winter, when the mixed layer deepens, temperature anomalies from the subsurface layer return to the ocean surface. Namias and Born (1970) were the first to describe this process. Alexander and Deser (1995) called this behavior of temperature anomalies in the upper ocean the “reemergence mechanism”. It occurs over large areas of the world’s oceans (Byju et al. 2018), but not all (de Coëtlogon and Frankignoul 2003; Sugimoto and Hanawa 2005; Frankignoul et al. 2021). Grist et al. (2019), using a high-resolution coupled ocean atmosphere model, studied the behavior of the temperature anomaly artificially

✉ Pavel A. Sukhonos  
pasukhonis@mail.ru

✉ Michael A. Alexander  
michael.alexander@noaa.gov

<sup>1</sup> Institute of Natural and Technical Systems, Sevastopol, Russia

<sup>2</sup> NOAA Physical Sciences Laboratory, Boulder, CO, USA

introduced under the mixed layer in the summer season and concluded that the sea surface temperature anomalies (SSTAs) reemergence in the North Atlantic has a significant impact on the winter climate of the Northern Hemisphere.

In order to examine the reemergence of temperature anomalies in the North Atlantic, Watanabe and Kimoto (2000) used a mixed layer model driven by daily atmospheric data generated by an atmospheric general circulation model, Zhao and Haine (2005) used a one-dimensional Lagrangian upper ocean model and Cassou et al. (2007) used atmospheric general circulation model coupled to a mixed layer ocean model and a thermodynamic ice model. These authors showed that winter-to-winter persistence of North Atlantic SSTAs exists in subpolar and midlatitude centers of action of the SSTA tripole associated with the North Atlantic Oscillation (NAO). Due to the reduced seasonality of the mixed layer, the recurrence is weaker in the subtropical tripole center. Cassou et al. (2007) also showed that the reemergence of the extratropical SSTA tripole occurs in November–December and lasts through the following spring. These authors noted that timing and intensity of the reemerging signal are a function of the depth of the winter mixed layer and the strength of the wintertime atmospheric forcing. Timlin et al. (2002) examined reemergence over the North Atlantic by performing empirical orthogonal functions (EOFs) analysis in the time–depth plane. These authors calculated the EOFs using seven depths (from 0 to 160 m) and 15 months from January to March of the following year during 1955–1995. de Coëtlogon and Frankignoul (2003) using monthly SSTAs showed that the regions of strong recurrence tend to coincide with the three centers of action of the North Atlantic SSTA tripole with an estimated timescale of 16 months. They found that the reemergence process could explain a large part of the observed interannual to decadal variability of the North Atlantic SSTA tripole. Sukhonos and Alexander (2023) using multiple datasets and EOFs decomposition showed that the dominant mode of interannual variability in the summer seasonal thermocline (~65–90 m in August–September) also has a tripole pattern. The tripole in the summer seasonal thermocline is most strongly related to SSTAs in the previous winter. During summer, the SSTA variance explained by this EOF decreases and in the subsequent autumn–winter, this value increases, reaching two-thirds of the initial signal.

An intense negative NAO phase at the beginning and end of 2010 contributed to the formation of the SSTA tripole pattern in the North Atlantic (Taws et al. 2011). Positive SSTAs (up to 1°C) were observed in the Labrador and Irminger seas and tropical latitudes (12–24° N), while negative SSTAs (from –0.5 °C to –1.5 °C) occurred in the western part of the subtropical gyre. Taws et al. 2011 found that the reemergence of winter temperature anomalies in the

upper layer of the North Atlantic contributed to the persistence of the negative NAO phase and the recurrence of conditions with abnormally low air temperatures in the winter of 2010–2011. Cassou et al. (2007) showed that reemerged SSTAs have a significant impact on the atmospheric model response favoring the same NAO phase that created them in the previous winter with a 15–20% positive feedback. Gastineau and Frankignoul (2015) applied the maximum covariance analysis technique to the 500-hPa geopotential height anomalies and SSTAs in the North Atlantic and showed that SST warming (cooling) in the subpolar and the eastern tropical North Atlantic leads a negative (positive) NAO phase during the fall and early winter. Thus, the SSTA tripole pattern in the North Atlantic, generated by the NAO variability, recurs in consecutive winters via the reemergence mechanism.

Ocean data are highly correlated in space and time. EOF decomposition is a traditional technique for studying large-scale patterns that explain much of the variability. However, significant correlation over time is not taken into account in traditional EOF analysis (Hannachi 2004). Extended empirical orthogonal functions (EEOF), an extension of the traditional EOF method, highlights temporal as well as spatial correlations in the data, including the evolution of patterns over time. EEOFs have been applied to climate data (e.g., Weare and Nasstrom 1982; Lau et al. 1992) including an analysis of the reemergence mechanism in the North Pacific Ocean (Alexander et al. 1999, 2001), which showed that the SSTAs in March–May are more strongly related to those in the following November–January than to the SSTAs in the intervening summer months, especially in the eastern part of the basin.

The study of the interaction between the main mode of atmospheric circulation and the intensity of the SSTA tripole reemergence in the North Atlantic can be done using the Granger causality technique (Granger 1969). The Granger quantification of causality is calculated as the improvement in the prediction of one variable when data for another is taken into account compared to the case without this consideration. In other words, one variable Granger causes another variable if it can be shown that the time series values of the first variable provide statistically significant information about the future values of the second variable. This technique has been used previously to identify the relationship between NAO and SST in the North Atlantic (Wang et al. 2004; Mosedale et al. 2006), NAO and winter sea ice variability in the Subpolar Atlantic (Strong et al. 2009), SST and Atlantic hurricane strength (Elsner 2007), and El-Niño/Southern Oscillation's impact on the Indian monsoon (Mokhov et al. 2011).

While the North Atlantic SSTA tripole reemergence has been studied in several observational and model studies, a

number of issues remain, including: (1) What part of the total upper ocean layer temperature variance is explained by the reemergence mechanism (both over the entire domain and in the centers action of the tripole)? (2) How is the SSTA reemergence in the centers of action of the tripole pattern formed and what is its relationship with the NAO and other parameters? In this study, we will investigate the evolution of temperature anomalies in the upper layer of the North Atlantic. For this purpose, we apply EEOFs to homogeneous and long-term data from three advanced ocean reanalyses. In contrast to previous studies, we will consider the evolution not of SSTAs, but of temperature anomalies in the upper ocean layer of the North Atlantic and all centers of action of the tripole structure.

## 2 Data and methods

We used three-dimensional monthly ocean temperatures and salinity, monthly zonal and meridional wind stress in the North Atlantic (15°–70° N 80°–8° W) from ocean reanalysis datasets, including the German contribution of the Estimating the Circulation and Climate of the Ocean project version 3S6m (GECCO3, 1°×1°, Jan 1948 – Dec 2018, 40 levels) (Köhl 2020), Ocean Reanalysis System 5 (ORA-S5, 1°×1°, Jan 1979 – Dec 2018, 75 levels) (Zuo et al. 2019) and Simple Ocean Data Assimilation version 3.12.2 (SODA3, 0.5°×0.5°, Jan 1980 – Dec 2017, 50 levels) (Carton et al. 2018). These reanalysis datasets were chosen because they represent well the association of tripole pattern in the summer seasonal thermocline with SSTAs in the North Atlantic (Sukhonos and Alexander 2023). Using TEOS-10 software (<http://www.teos-10.org/>), density profiles were calculated from temperature and salinity profiles from these reanalyses. A density difference of 0.125 kg/m<sup>3</sup> between the ocean surface and the bottom of ocean mixed layer was used as the criterion to determine the mixed layer

depth (MLD) (Monterey and Levitus 1997). Monthly averages of the NAO index for the period 1950–2021 were taken from the website of the National Center for Climate Prediction, USA (<https://www.cpc.ncep.noaa.gov/products/precip/CWlink/pna/nao.shtml>).

To remove low-frequency variability, third-order polynomials were first subtracted from the time series of the GECCO3 data at each grid point and the NAO index. From the ORA-S5 and SODA3 time series, only first-order polynomials (linear trends) were subtracted because of their short duration. The polynomial coefficients were calculated by the least-squares method. The filtering removes the influence of the long-term increase in ocean temperature (primarily due to the increase in greenhouse gases) and the Atlantic Multidecadal Oscillation.

Further, the monthly temperature anomalies are calculated by removing the average long-term temperature values for each calendar month. This filtering removes the influence of the seasonal cycle. The next step is to normalize the temperature anomalies for the EEOF calculation so all levels and months are weighted equally. For each calendar month, the average standard deviation (SD) of temperature anomalies at all grid points in the domain for the entire period at each level was calculated. Then, the temperature anomalies at each grid point in the domain for each month at each level are dimensionless by normalizing them to their average basin-wide SD. The outlined procedure normalizes temperature anomalies both in depth and in season.

The values of the temperature SD in the 0–300 m layer averaged over the North Atlantic domain are shown in Fig. 1. Near the surface (6 m for GECCO3, 0.5 m for ORA-S5 and 5 m for SODA3), the SD values range from minimum in February (0.45 °C for GECCO3 and ORA-S5, 0.55 °C for SODA3) to maximum in July (0.65 °C for GECCO3 and ORA-S5, 0.75 °C for SODA3). In the summer seasonal thermocline (~65–90 m in August–September), there is a subsurface SD maximum, with values of more than 0.6°C for

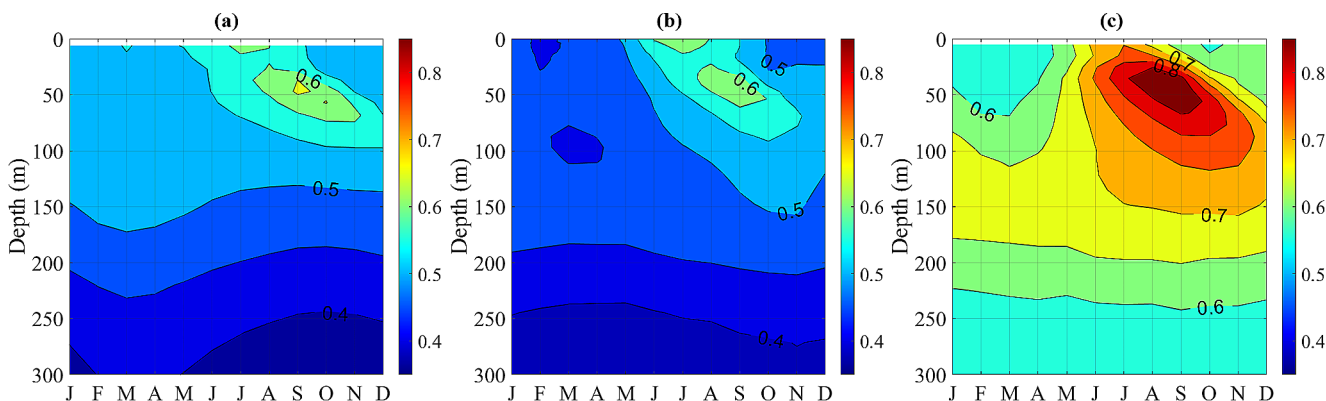


**Fig. 1** Average SD of the North Atlantic (15°N–70°N) ocean temperature in each month at each level in the 0–300 m layer are presented from the GECCO3 dataset for the years 1948–2018 (a), the ORA-S5

dataset for the years 1979–2018 (b) and the SODA3 dataset for the years 1980–2017 (c). Contour interval is 0.05 °C

GECCO3 and ORA-S5, 0.8 °C for SODA3. The SD values decrease with depth; below 200 m, these values are less than 0.45 °C for GECCO3 and ORA-S5, and 0.65 °C for SODA3 in all months of the year. The GECCO3 and ORA-S5 datasets have the same spatial resolution. However, there are some differences between the reanalyses. The GECCO3 SD values exceed 0.5°C in the 0–122.5 m layer in all months, while they only exceed 0.5°C in the 0–97 m layer during the second half of the year in ORA-S5. These differences are partly due to different length of the time series. In addition, due to its higher spatial resolution, the temperature SD values in SODA3 are ~30% higher than in the other datasets. In general, the SD structure with a pronounced summer thermocline in the North Atlantic 0–300 m layer is similar in these datasets.

To optimize the EEOF analysis for isolating the reemergence mechanism, we formed the covariance matrix as follows. We took all grid points in the spatial domain for January of the first year, and then concatenated to the covariance matrix all grid points in the spatial domain for February of the first year, then March of the first year, and so on through April of the second year. Thus, there are 16 months of values in this first time period. Then we repeated the same from January of the second year to April of the third year and so on. The covariance matrix includes temperature anomalies at all levels available in the 0–300 m layer. So, the evolution of monthly temperature anomalies in this layer given by the EEOF matrix. The leading EEOF of monthly temperature anomalies from January through the following April (lags of 0–15 months) in the 0–300 m layer is computed from the covariance matrix described above. This EEOF displays the leading pattern of the seasonal evolution of temperature anomalies in the upper 300 m. The first extended principal component (EPC1) indicates how the amplitude and phase of this pattern varies from one year to the next (actually 16 month period). An example of this procedure for representing the evolution of the reemergence in three dimensions is shown in (Alexander et al. 1999). Since the basin average SD within the domain varies only slightly in all months (see Fig. 1), the normalized and non-normalized EEOF1 (not shown) are very similar. The lower boundary of the considered layer was chosen so that the explained variance of the reemerging signal was maximized. When the lower boundary was chosen to be at a greater depth, the explained variance of the reemerging signal sharply decreased, since the reemerging signal does not penetrate beyond ~300 m.

The percentage of variance of temperature anomalies, explained by the time coefficient of the leading EEOF (EPC1), is computed using

$$\sum_{i=1}^N r_i^2 \sigma_i^2 / \sum_{i=1}^N \sigma_i^2, \quad (1)$$

where  $r$  is the correlation coefficient between the time series of temperature anomalies and the EPC1,  $\sigma$  is the standard deviation of the temperature anomalies,  $i$  indicates an individual grid point, and  $N$  is the total number of grid points.

Testing for causality and possibly feedback between NAO and EPC1 is based on the concept of «Granger causality». This technique was first implemented by Granger (1969) for stationary Gaussian processes. Since this technique uses regression models, the time series were examined for normality and stationarity before the Granger analysis. The Shapiro–Wilk goodness-of-fit test (Shapiro and Wilk 1965) confirmed the normality of NAO and EPC1 values. Four tests for stationarity were used sequentially to ensure the reliability of the results: Augmented Dickey–Fuller test, Phillips–Perron test, Kwiatkowski, Phillips, Schmidt and Shin (KPSS) test, Variance ratio test for random walk. The first three tests show that all time series are stationary, except for the NAO in March and August and GECCO3 EPC1 based on results of the KPSS test. The fourth test shows that the NAO from January to November is a random walk process. In general, the time series used, the  $NAO_t$  and  $EPC1_t$ , can be considered stationary. Such a process is uniquely described by a two-dimensional linear vector autoregression model given by Eqs. (2) and (3):

$$NAO_t = \sum_{k=1}^{\infty} a_{NAO,k} NAO_{t-k} + \sum_{k=1}^{\infty} b_{NAO,k} EPC1_{t-k} + \xi_t \quad (2)$$

and

$$EPC1_t = \sum_{k=1}^{\infty} a_{EPC1,k} EPC1_{t-k} + \sum_{k=1}^{\infty} b_{EPC1,k} NAO_{t-k} + \psi_t \quad (3)$$

where  $a$ ,  $b$  are regression coefficients;  $\xi_t$ ,  $\psi_t$  – noise residuals in the regression, representing zero-mean Gaussian white noise with corresponding component variances  $\sigma_{\xi}^2$  and  $\sigma_{\psi}^2$ . The condition that the noise is «white» is equivalent to the minimum prediction error (Box and Jenkins 1976), while  $\sigma_{\xi}^2 = \sigma_{NAO,jo}^2$  and  $\sigma_{\psi}^2 = \sigma_{EPC1,jo}^2$ . Further, the  $NAO_t$  process also obeys the one-dimensional autoregressive equation, i.e., Eq. (2) with zero coefficients  $b_{NAO,k}$  and white noise  $\xi_t$ , the variance of which is  $\sigma_{\xi_t}^2 = \sigma_{NAO,ind}^2$ . Then, according to the noise variances  $\sigma_{\xi}^2$ ,  $\sigma_{\xi_t}^2$ , the magnitude of the prediction improvement  $G_{EPC1 \rightarrow NAO}$  is determined. The normalized prediction improvement value  $G_{EPC1 \rightarrow NAO} = (\sigma_{NAO,ind}^2 - \sigma_{NAO,jo}^2) / \sigma_{NAO,ind}^2$  characterizes Granger causality in the  $EPC1 \rightarrow NAO$  direction. This value, expressed as a percentage, shows how much the noise variance (prediction error) in the joint model (i.e., taking into account the additional process) is reduced compared to the noise variance in the individual model (i.e., without taking into account the additional process). The normalized prediction improvement value  $G_{NAO \rightarrow EPC1}$  is determined similarly.

To estimate the theoretical values of  $G_{EPCI \rightarrow NAO}$  and  $G_{NAO \rightarrow EPCI}$  over a finite time series, all sums in Eqs. (2) and (3) are restricted to the term  $k=p$  (instead of  $k = \infty$ ), and the noise coefficients and variances in the corresponding vector autoregressive models of order  $p$  are estimated using the standard least squares method. When analyzing climatic time series, the Schwarz criterion (Schwarz 1978) is used to select the order. The optimal model of the NAO process is chosen to minimize the value  $S_{NAO} = \frac{N}{2} \ln \sigma_{NAO,ind}^2 + \frac{k}{2} \ln N$ , where  $k$  is the number of estimated coefficients,  $N$  is the length of the series. Next, it is necessary to check the adequacy of the resulting autoregressive model for a fixed  $k$ . If the individual model is not satisfactory, then the value of  $k$  should be increased. For the purpose of identifying a causal relationship, it is more appropriate to select the value of  $k$  that provides the maximum of the prediction improvement value  $G_{EPCI \rightarrow NAO}$ . Then the adequacy of the constructed joint autoregressive model is checked and, if necessary, the selected value of the model order is changed. The trial order values of the individual and joint models should vary in such a range that the number of coefficients of any autoregressive model used is significantly less than  $N$ . As a rough estimate, it should not exceed  $\sqrt{N}$ , i.e. approximately 8 (6) for GECCO3 data (ORAS5 and SODA3 data). Similarly, individual orders and degrees were selected for the EPCI process. The statistical significance of the difference between the  $G_{EPCI \rightarrow NAO}$  and  $G_{NAO \rightarrow EPCI}$  scores from zero is checked using Fisher's F-test (Seber and Lee 2012).

### 3 Results

#### 3.1 Basin-wide analysis

The percent variance explained by EEOF1 in each month from January through April of the following year (16 month period) as a function of depth, calculated by Eq. (1), is shown in Fig. 2. In the first winter (from January through April), ~13% of the monthly variance is concentrated in the 0–100 m layer. In the following winter (from December through February of the following year), approximately 8–9% of the monthly variance is concentrated in the 0–100 m layer, i.e., about 2/3 of the initial variance. The leading pattern practically disappears at the surface in summer, since in August–September it explains only 4% of the variance, while 12–14% of the variance remains in the summer seasonal thermocline. Below 200 m ~10% of the monthly variance remains from July to December in GECCO3 and ~6% in ORA-S5. The reemerging signal appears to extend deeper in GECCO3 relative to the other two datasets. The percentage values according to SODA3 are ~2/3 of those from the other datasets (Fig. 2c). However, for SODA3, the reemerging signal can still be seen in the upper 300 m. Overall variance explained by EEOF1 averaged over all months and depths is ~10% for GECCO3, ~9.2% for ORA-S5 and ~5.6% for SODA3 of the total variance. The relatively low percent variance explained may result from reemergence varying over the large North Atlantic domain, with regional changes in timing and vertical structure, as well as small regions in which reemergence does not occur. Thus, all datasets show the reemergence process although its representation varies between them.

The EPCI time series obtained from the three datasets are similar to each other (Fig. 3a). The synchronous correlation coefficient for these time series in the overlapping period equals 0.65 for GECCO3–ORA-S5, 0.62 for

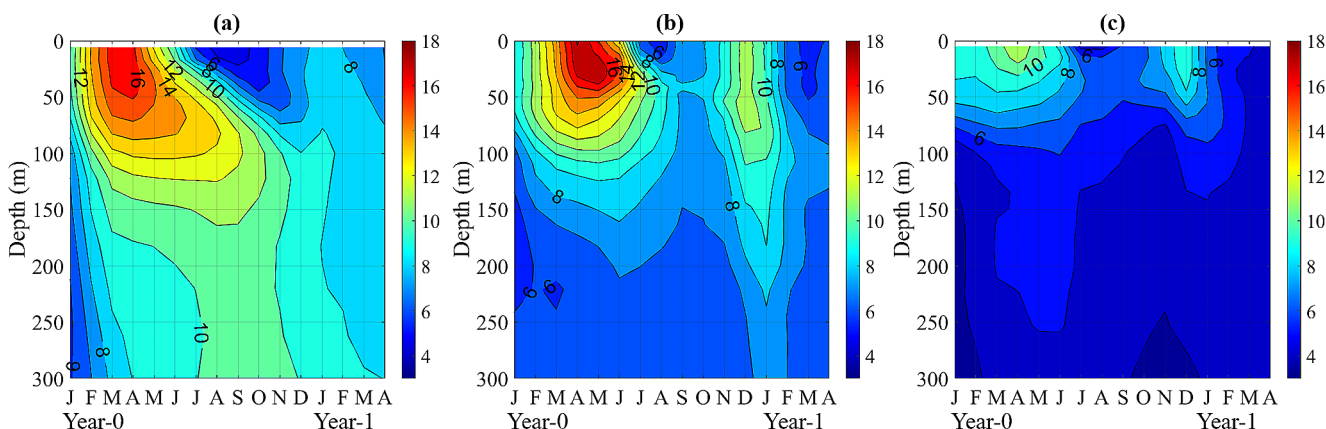


**Fig. 2** The percent variance of monthly temperature anomalies in the 0–300 m layer explained by EEOF 1 for the North Atlantic domain (15°N–70°N) from GECCO3 (a), ORA-S5 (b) and SODA3 (c) datasets

when it is computed as a function of both time and depth. Results are presented for each month from January through April of the following year

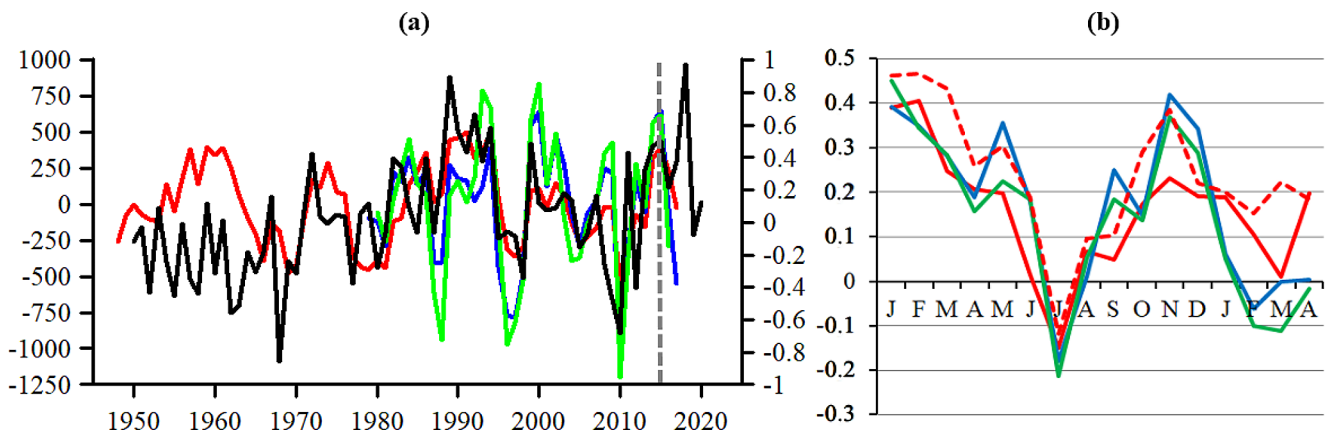


**Fig. 3** (a) Extended PC1 time series from GECCO3 (red), ORA-S5 (blue) and SODA3 (green) datasets and the NAO index averaged from January to April of the following year (black, scale on the right) for the available years; (b) Correlation coefficients between the extended

PC1 and the NAO index from previous January to following April for the available period. Dashed red line on (b) denotes correlation with GECCO3 data for the period 1979–2017. The vertical dashed gray line on (a) represents 2014

**Table 1** Granger causality characteristics between the time series of the NAO index from January to April of the following year and EPC1 in the data used. The down arrow indicates a unidirectional positive relationship between NAO and EPC1, significant at the 97.5% confidence level

dataset	period	NAO index							
		JAN	FEB	MAR	APR ... OCT	NOV	DEC	JAN2 ... APR2	
GECCO3	1951–2017	↓	↓	↓					
	1979–2017	↓	↓	↓		↓			
ORAS5	1979–2017	↓	↓	↓			↓		
SODA3	1980–2016	↓	↓	↓			↓		
		EPC1							

The double arrow signifies a bidirectional positive relationship between NAO and EPC1, significant at the 90% confidence level

GECCO3–SODA3 and 0.91 for ORA-S5–SODA3. There are 15 levels in the layer 0–300 m in GECCO3 data (35 levels in ORA-S5 data and 21 levels in SODA3 data). Higher vertical resolution makes it possible to more accurately describe the behavior of temperature anomalies in upper 300 m and thus may more accurately depict the reemergence process, expressed by EPC1. This may explain the higher correlation between EPC1 from ORA-S5 and SODA3 than the correlation between EPC1 from GECCO3 and EPC1 from other reanalyses. The EPC1 time series for the North Atlantic domain have an absolute minimum in 2010. Figure 3a also shows the NAO index, the values of which are averaged from January through April of the following year. Sliding correlation between the values of averaged NAO index and EPC1 from GECCO3 data with a window width of 31 years (the value in 1965 was obtained for the period 1950–1980, the value in 1966 was obtained for the period 1951–1981 and so on) is positive. The correlation coefficients before 1975 are less than 0.4, but after 1979 they are greater than 0.7. This confirms the strong relationship between the temporal evolution of the reemergence process in the upper North Atlantic Ocean and the interannual variability of the main atmospheric circulation mode over the North Atlantic – NAO, which also rapidly switched to the

opposite phase in 2010 (Taws et al. 2011; and references therein). In the first two decades (1950–1970), this relationship was not strongly pronounced, which may be due to the low quality and quantity of ocean data and the presence of decadal variability in the reemergence process.

The correlations between EPC1 in the North Atlantic and the NAO index for each month are shown in Fig. 3b. The GECCO3 values were compared for two periods: 1948–2017 and 1979–2017. For the second period, somewhat higher correlation coefficients were obtained, close in magnitude to the two other datasets. In general, the relationship with the NAO index is similar for all datasets. The correlations are high and positive in January–February (about 0.4–0.5), near zero (from –0.2 to 0.2) from April to September, and then positive again in November–December (about 0.35–0.4). Thus, the temporal variability of the NAO index and the configuration of the SSTA tripole pattern in the North Atlantic in the first and subsequent winters are consistent.

Granger causality characteristics between the time series of the NAO index from January to April of the following year and EPC1 from Fig. 3a are shown in Table 1. All data used indicate a unidirectional relationship between NAO in the first winter and EPC1. This relationship is significantly

positive at the 97.5% confidence level. The identified impact of NAO on EPC1 in January–March indicates that EPC1 responds to NAO changes without delay. The intensification of NAO leads to an increase in EPC1. The effect of EPC1 on NAO is not manifested in the first winter. Statistically significant and most strongly the influence of NAO on EPC1 is expressed in January–March of the first year. When the NAO values in these months are taken into account in the joint model, the noise variance, which indicates the error of EPC1 prediction, is reduced by 25% in GECCO3 1951–2017 data (29% in GECCO3 1979–2017 data), 23% in ORAS5 data, and 28% in SODA3 data. In the first winter, the NAO forms the SSTA tripole in the North Atlantic, the amplitude of which determines the intensity of the SSTA tripole reemergence process.

In the period from April to October of the first year and from January to April of the second year, the values of  $G_{EPC1 \rightarrow NAO}$  and  $G_{NAO \rightarrow EPC1}$  for any non-zero  $p$  are not statistically significantly different from zero according to the  $F$ -test, i.e., the relationship between the NAO index in these months and EPC1 not noted.

Based on the analysis of the time series of the NAO index in November and EPC1 in GECCO3 data for the period 1979–2017 and the NAO index in December and EPC1 in ORAS5 and SODA3 data, the Granger analysis indicates that positive prediction improvements were obtained in both directions and significantly different from zero at the 90% confidence level according to the  $F$ -test. Taking into account the influence of the NAO in November (EPC1) on EPC1 (the NAO in November) joint model, the noise variance (prediction error) is reduced by 15% in GECCO3 data in the period 1979–2017. Taking into account the influence of the NAO in December (EPC1) on EPC1 (the NAO in December) joint model, the noise variance is reduced by 18% in ORAS5 data. The indicated noise variance is reduced by 14% in the SODA3 data. NAO index anomalies cause EPC1 anomalies with the same sign, and EPC1 anomalies, in turn, also cause NAO index anomalies with the same signs. This positive feedback process occurs simultaneously. Moreover, the temperature anomalies that reemerged from the subsurface layer in November–December contribute to a change in the large-scale atmospheric circulation toward the NAO phase that formed these anomalies. This conclusion is consistent with the results of model studies for the extratropical oceanic thermal anomalies (Cassou et al. 2007; Grist et al. 2019).

When using the GECCO3 data for the entire period 1948–2017, the  $G_{EPC1 \rightarrow NAO}$  and  $G_{NAO \rightarrow EPC1}$  were not significant but a significant at the 97.5% confidence level unidirectional relationship  $G_{NAO \rightarrow EPC1}$  was obtained in the first winter for the period 1951–2017. Perhaps this is due to the low quality of the reanalysis in the years from 1948 to 1950, when a

small number of observations were available. The analysis for the period 1979–2017 confirms these findings and provides significant estimates of the bidirectional relationship in November. While other reanalyses used give significant estimates of the bidirectional relationship in December. The correlation between the values of the NAO index in November and December in the period 1951–2017 (1979–2017) is 0.37 (0.69). The similarity of the NAO index temporal variability in these months and the similarity of the EPC1 temporal variability from different datasets (Fig. 3a) give reason to believe that the positive feedback actually exists in November–December, regardless of the dataset.

The evolution of the leading pattern of temperature variability is presented in Fig. 4 as correlations between the EPC1 with the time series of monthly temperature anomalies at individual grid points in the North Atlantic domain. The correlation maps are shown for every other month from January through April of the following year according to the GECCO3 data for the ocean surface (6 m) and subsurface layer (summer seasonal thermocline, 68.5 m). The results from the other datasets and alternate months are similar (not shown). With a time series length of about 70 years, a correlation coefficient of 0.4 or more can be considered significant at the 99% confidence level. The leading pattern during the entire 16-month period is a tripole structure with anomalies of the same sign in the tropical and high latitudes of the North Atlantic and of the opposite sign in the subtropical gyre. In the first winter, with a deep mixed layer, the regions with high correlations in absolute value are large. The location of these regions on the ocean surface and in the subsurface layer coincides. The greatest correlations are found in March, when the mixed layer has its maximum depth over most of the North Atlantic. The value of correlations in the inner part of the subtropical and subpolar gyres exceeds 0.8 in absolute value in this month. In May, the regions with high correlations in absolute value on the ocean surface decrease, while in the subsurface layer these regions remain the same as in March. From June to September, the regions with high correlations in absolute value on the ocean surface are minimal. The tripole structure of temperature anomalies persists in the summer seasonal thermocline (~65–90 m). The magnitudes of the correlations between EPC1 and temperature anomalies at 68.5 m in the centers of action of the tripole structure exceed 0.6 in absolute value. In the following winter (from November to March of the following year), areas of positive and negative correlations emerge on the ocean surface and form a tripole structure. These regions are located above the regions of high correlations in the subsurface layer. Thus, the North Atlantic SSTAs tripole structure in March–April is more strongly associated with the SSTAs tripole structure in December–January of the following year than with SSTAs in the intervening summer months. During

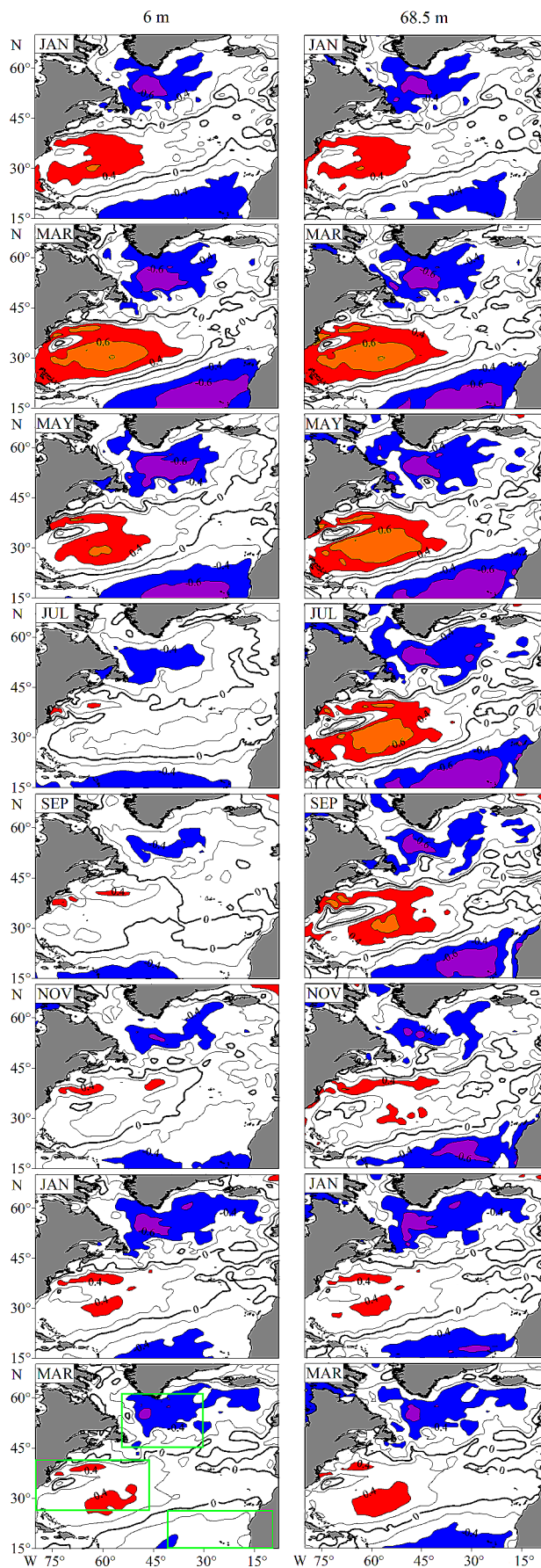


**Fig. 4** The evolution of the leading pattern of temperature variability over  $15^{\circ}\text{N}$ – $70^{\circ}\text{N}$  in the North Atlantic as indicated by EEOF1 of monthly temperature anomalies on the surface (left panel) and in the 68.5 m level (right panel) from January through April of the following year. The results are presented as the correlation between the principal component (time series) of EEOF1 with the temperature anomalies at the individual grid points for every other month beginning in January (the other months which are not shown indicate a similar evolution). Results are presented for the GECCO3 dataset for the years 1948–2017. The contour interval is 0.2 with values  $>0.4$  ( $>0.6$ ) shaded red (orange) and those  $<-0.4$  ( $<-0.6$ ) shaded blue (purple). Regions HIGH, MID, and LOW are shown in lower left figure by green rectangles

these months, the tripole structure is well distinguished in the subsurface layer.

### 3.2 Regional analysis

The basin-wide analysis showed that the reemergence mechanism occurs over much of the North Atlantic (see Figs. 2 and 4). Here we focus on the vertical structure of the reemergence mechanism at the centers of action of the North Atlantic SSTA tripole pattern. Three areas are defined by the leading EEOF pattern: one off the east coast of the United States and two of the opposite sign south of Greenland and in the eastern Subtropical Atlantic. To obtain a clear picture of the reemergence process, rectangular areas were selected in the north ( $45^{\circ}\text{N}$ – $61^{\circ}\text{N}$   $55^{\circ}\text{W}$ – $30^{\circ}\text{W}$ ), central ( $25^{\circ}\text{N}$ – $40^{\circ}\text{N}$   $80^{\circ}\text{W}$ – $47^{\circ}\text{W}$ ) and south ( $15^{\circ}\text{N}$ – $25^{\circ}\text{N}$   $40^{\circ}\text{W}$ – $10^{\circ}\text{W}$ ) parts of the region under consideration, indicated as HIGH, MID and LOW, respectively.

All three regions show signs of a reemergence mechanism in the three reanalyses. As an example, the pattern of the reemergence process in GECCO3, based on the percent variance explained by EEOF1, is shown in Fig. 5. Different number of layers was used in each region as the extent of the winter mixed layer and the reemergence process decreases with latitude. EEOF/EPC1 are calculated with Eq. (1) separately for each region using temperature anomalies at all levels down to depths 1200 m, 350 m, 120 m in the HIGH, MID and LOW regions, respectively. The structure and timing of the leading pattern differ in the three locations. The overall variance explained by EEOF1 in the HIGH region in each month and 0–650 m layer is 19.5% for GECCO3 (17.4% for ORA-S5 and 8.8% for SODA3) of the total variance. The maximum of the reemergence signal with an explained variance of  $>30\%$  for GECCO3 ( $>25.4\%$  for ORA-S5 and  $>6.7\%$  for SODA3) is located in the 180–420 m layer from August to November. Since the maximum variance explained is very deep in the HIGH region, not all of that signal returns to the surface and thus is not part of the reemergence process. Therefore, the 0–300 m layer is well suited for basin-wide EEOF analysis. The strong return of SSTAs formed in the previous winter can be associated with deep convection penetrating to depths



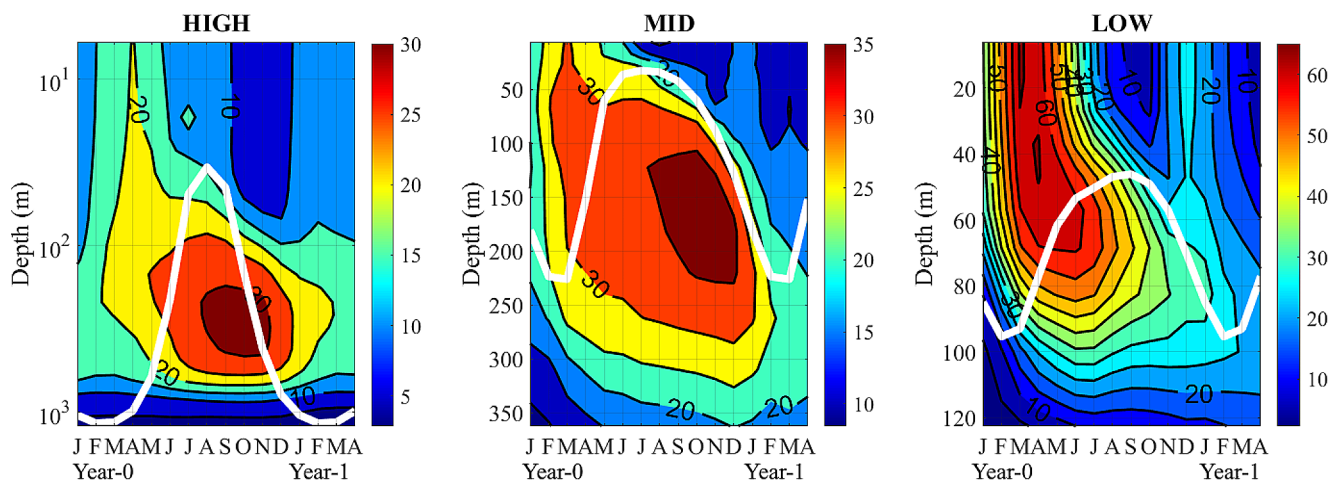


**Fig. 5** The percent variance of monthly temperature anomalies explained by EEOF 1 for three centers action of the North Atlantic tripole pattern HIGH (45°N–61°N 55°W–30°W, 0–1200 m), MID (25°N–40°N 80°W–47°W, 0–350 m) and LOW (15°N–25°N 40°W–10°W, 0–120 m) from the GECCO3 dataset when it is computed as a function of both time and depth. A different depth and color

scale is used for each action center. The isolines in all figures are drawn through 5%. Results are presented for each month from January through April of the following year. The white–solid lines denote climatological MLD in the considered regions. The vertical axis in the graph for the HIGH region is plotted on a logarithmic scale

of 1–2 km during the cold season in the Subpolar Atlantic (Marshall and Schott 1999; Deser et al. 2003). The overall variance explained by EEOF1 in the MID region in each month and 0–350 m layer is 24.1% for GECCO3 (19.4% for ORA-S5 and 6.5% for SODA3) of the total variance. The maximum of the reemergence signal with an explained variance of >35% for GECCO3 (>18.6% for ORA-S5 and >6.7% for SODA3) is located in the 100–220 m layer from July to December. The overall variance explained by EEOF1 in the LOW region in each month and 0–120 m layer is 30.9% for GECCO3 (26.6% for ORA-S5 and 17.2% for SODA3) of the total variance. A pronounced maximum of the reemergence signal in the subsurface layer in the summer months is not observed. In the first winter (from January to April) 44.9% for GECCO3 (42.2% for ORA-S5 and 32.3% for SODA3) of the monthly variance is concentrated in the 0–100 m layer. In the next winter (from December to February of the next year) 24.3% for GECCO3 (20.9% for ORA-S5 and 13.7% for SODA3) of the monthly variance is concentrated in the 0–100 m layer, i.e., about 1/2 of the initial variance. The leading pattern disappears at the surface in summer, since in August–September it explains less than 10% of the variance. There is no signal of the SSTA reemergence in the LOW region below 120 m. The reemergence pattern in the LOW region looks very much like a “classical” reemergence signal.

Thus, the EEOF technique shows that the SSTA reemergence mechanism exists in all three centers of action of the tripole pattern, but with clear differences between them. In the HIGH region, the SSTAs spread within the deep mixed layer in spring, remain in the 100–650 m layer in summer–autumn, and then partly reemerge at the surface 2–3 months

later than in the other two areas. In the MID region, SSTAs decrease in the spring but temperature anomalies remain in a layer of 70–270 m in summer–autumn and then return to the surface in December–January. In the LOW region, in contrast to the other two regions, the reemerging signal has a maximum in spring of the first year, which occurs within the mixed layer, remains in the 45–100 m layer in summer–autumn, and then about half of the signal returns to the surface in December. Differences in the time and strength of the reemerging signal are largely due to the regional amplitude of the average seasonal cycle of the MLD. Zhao and Li (2010) also note that in the North Atlantic, the SSTA reemergence occurs later north of 30°N and earlier south of this latitude. In the North Atlantic, the maximum winter MLD increases from ~70–100 m in tropical latitudes to ~1–2 km in convective regions at high latitudes. Therefore, the depth to which temperature anomalies penetrate in winter–spring increases poleward. When the upper mixed layer deepens in the next autumn–winter, temperature anomalies located at shallower depths reach the ocean surface earlier.

Composite values of the NAO index and temperature anomalies during periods when the EPC1 values exceed ±1 SD in absolute value in three centers of action of the tripole pattern are shown in Fig. 6. In 16–month periods from January through April of the following year when EPC1 values exceed +1 SD (14 periods for 1948–2017 in the GECCO3 data), a tripole pattern is formed on the ocean surface during the first winter, corresponding to the NAO positive polarity. During these periods, the NAO index values from January to April and from November to January of the following year are significantly positive at the 99% confidence level. The SSTA composite values in the HIGH, MID and LOW

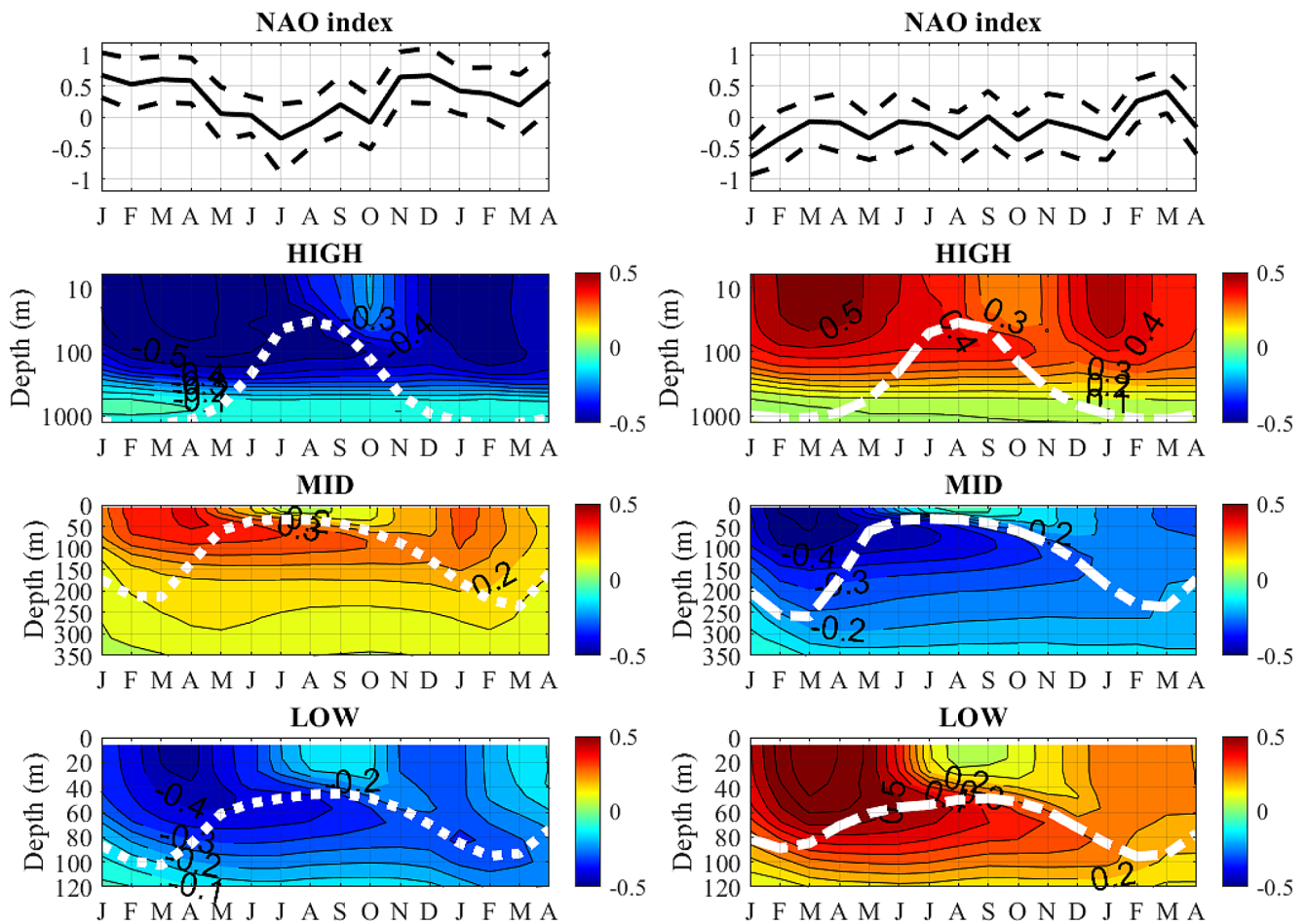


**Fig. 6** Composites of the NAO index and temperature anomalies in 16-month periods from January through April of the following year when EPC1 values  $> +1SD$  (left panel) and when EPC1 values  $< -1SD$  (right panel) in the three centers of action of the North Atlantic tripole pattern HIGH ( $45^{\circ}N$ – $61^{\circ}N$   $55^{\circ}W$ – $30^{\circ}W$ , 0–1300 m), MID ( $25^{\circ}N$ – $40^{\circ}N$   $80^{\circ}W$ – $47^{\circ}W$ , 0–350 m) and LOW ( $15^{\circ}N$ – $25^{\circ}N$   $40^{\circ}W$ – $10^{\circ}W$ , 0–120 m) from the GECCO3 dataset. The dashed lines

on upper panels indicate the boundaries of the 99% confidence interval. Composite temperature anomaly exceeding  $0.25^{\circ}C$  in absolute value is significant at the 99% confidence level. Isolines are drawn through  $0.05^{\circ}C$ . The white short-dashed and long-dashed lines are the MLD during these periods. Please note the same color scale in all figures. The vertical axis in the graphs for the HIGH region is plotted on a logarithmic scale

regions in the first winter are  $-0.55^{\circ}C$ ,  $0.4^{\circ}C$  and  $-0.45^{\circ}C$ , respectively. The MLD in the HIGH region in February–March is deeper than the depth to which the reemerging signal extends, but it is consistent with Fig. 5. In 16-month periods from January through April of the following year when EPC1 values are less than  $-1$  SD (13 periods for 1948–2017 in the GECCO3 data), a tripole pattern corresponding to the NAO negative polarity is formed on the ocean surface during the first winter. The NAO index values in January of the first year are significantly negative at the 99% confidence level. The SSTA composite values in the HIGH, MID and LOW regions in the first winter are  $0.5^{\circ}C$ ,  $-0.5^{\circ}C$  and  $0.6^{\circ}C$ , respectively. In all three regions and for both composites, the temperature anomalies formed in the deep mixed layer in the first winter, remain in the subsurface layer (under the upper mixed layer) in summer, and reemerge on the ocean surface in the autumn–winter when

the upper mixed layer deepens again. This behavior of temperature anomalies is fully consistent with the upper mixed layer dynamics and corresponds to the concept of reemergence. For all three regions, the MLD composite values in the first winter with negative SSTAs are greater than with a positive SSTA, while in summer the MLDs are shallower. An explanation of this phenomenon will be given below using the LOW region as an example.

Let us consider how the SSTA reemergence mechanism in the LOW region interact with the MLD and wind stress from the previous January through April of the following year (Fig. 7). The regional EPC1–MLD correlations are negative from January to May with a maximum absolute value in February–March (about  $0.55$ – $0.6$ ) and positive from June to April of the following year with a maximum absolute value in August–September (about  $0.35$ – $0.45$ ) (Fig. 7a). The transition from a negative correlation between

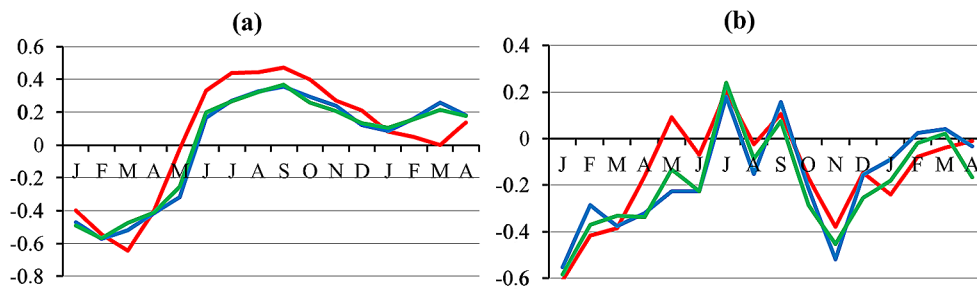


**Fig. 7** Correlation coefficients between the regional EPC1 of the EEOF 1 and the MLD (a), wind stress modulus (b) from previous January to following April in the subtropical center action of the North Atlan-

tic tripole pattern (15°N–25°N 40°W–10°W), which is denoted as the LOW region, from GECCO3 (red), ORA-S5 (blue) and SODA3 (green) datasets

**Table 2** Average values  $\pm 1$  SD of the NAO index and the SSTA, MLD and wind stress according to the datasets used in the LOW region in January of the first year reemergence, when the values of regional EPC1 exceed  $\pm 1$  SD in absolute value

	NAO index	Dataset	SSTA, °C	MLD, m	Wind stress, N/m <sup>2</sup>
EPC1 < -1 SD	<b>0.67 ± 0.36</b>	GECCO3	<b>-0.34 ± 0.24</b>	87 ± 8	<b>0.13 ± 0.03</b>
		ORA-S5	<b>-0.53 ± 0.14</b>	<b>97 ± 6</b>	<b>0.13 ± 0.02</b>
		SODA3	<b>-0.55 ± 0.25</b>	<b>90 ± 6</b>	<b>0.12 ± 0.02</b>
EPC1 > +1 SD	<b>-0.64 ± 0.29</b>	GECCO3	<b>0.44 ± 0.21</b>	81 ± 3	<b>0.06 ± 0.02</b>
		ORA-S5	<b>0.52 ± 0.25</b>	<b>75 ± 4</b>	<b>0.07 ± 0.01</b>
		SODA3	<b>0.61 ± 0.28</b>	<b>73 ± 3</b>	<b>0.06 ± 0.01</b>

Significant values at the 99% confidence level are in bold

regional EPC1 (EEOF analysis performed only for the LOW region) and MLD anomalies in the winter season to a positive correlation in the subsequent autumn–winter season is consistent with the MLD seasonal variation and the reemergence mechanism (Alexander et al. 2001). A negative SSTA formed in the first winter (in the LOW region with the NAO and wind stress intensification) makes the surface water denser and as a result, the MLD increases. This temperature anomaly in the subsurface layer in summer, leads to an increase in water density (neglecting the contribution of salinity) under the upper mixed layer and increases vertical stratification in the summer thermocline. It results in less deepening of the upper mixed layer in the subsequent summer–autumn for the same amount of atmospheric forcing. The regional EPC1–wind stress modulus correlations in the LOW region are shown in Fig. 7b. In the winter of the first year, the correlations are negative with a maximum absolute value of 0.55–0.6 in January. Then from May to September the correlations have near-zero values (–0.2 to 0.2). In the second winter, the correlations are negative with maximum absolute values of about 0.35–0.5 in November–December. The correlations are low in January–April of the following year. An increase in the wind stress modulus, consistent with the NAO variability, leads to the formation of a negative SSTA in this region in the first winter. The negative SSTA reemergence in November–December is consistent with an increase in concurrent wind stress modulus in this region. Note the high consistency of the regional EPC1–wind stress modulus correlations in the LOW region (Fig. 7b) and the

correlations between the NAO index and EPC1 calculated for the entire North Atlantic (Fig. 3b). This confirms that the relationship between the SSTA reemergence and the NAO variability is similar both for the subtropical center of action and for the entire tripole. A significant concurrent regional EPC1–wind stress correlation extremum in November–December, coinciding in sign with the correlation extremum in January of the first year of reemergence, suggests that reemerged SSTAs in this month act to maintain the same NAO phase that formed them in the previous winter.

To confirm the regional EPC1–MLD and regional EPC1–wind stress relationships in the LOW region, we estimated the values of these parameters in years when the regional EPC1 magnitude exceeded  $\pm 1$  SD (Table 2). In these years, the SSTA signs in February and November–December and the temperature anomalies below the lower upper mixed layer boundary from March to August coincide (Fig. 6). During the formation of a negative (positive) SSTA (with an absolute value of about 0.35–0.5 °C) in January in the LOW region, which undergoes reemergence to the next winter, the NAO index is positive (negative), the wind speed is enhanced (weakened) and upper mixed layer is deeper (shallower). The exact magnitudes of these anomalies vary across datasets used. However, analyzing all the datasets, the composite anomalies of MLD and wind stress are ~10% and ~30% of their average values in January, respectively. In addition, negative correlations with the regional EPC1 are noted in November (they are significant at the 90% confidence level for wind stress and the NAO index). The reemerging negative

SSTAs in the LOW region are accompanied by composite wind stress values of  $0.09 \pm 0.01 \text{ N/m}^2$  for GECCO3 and  $0.08 \pm 0.01 \text{ N/m}^2$  for ORA-S5 and SODA3, and NAO index values of  $0.51 \pm 0.42$  in November. The reemerging positive SSTAs in the LOW region are accompanied by composite wind stress values of  $0.06 \pm 0.01 \text{ N/m}^2$  for all datasets, and NAO index values of  $-0.45 \pm 0.39$  in November. In the reemergence years the composite anomalies of wind stress are  $\sim 15\%$  of their average values in November. The differences between these composite anomalies are significant at the 90% confidence level. This may indicate a moderate positive relationship between the reemergence process and changes in the wind stress fields in the LOW region, i.e. that the reemerging signal of negative (positive) SSTA, created during the enhanced (weakened) wind stress in January, can lead to an additional intensification (weakening) of the wind stress in November. Note that the relatively low correlation values indicate that other processes in the second winter, e.g., the impact of surface heat fluxes and wind stress, are also important (Alexander et al. 2000; Junge and Haine 2001; Zhao and Haine 2005).

To illustrate the relationship of reemerging ocean temperature anomalies with a repeat NAO, we present the variability of the NAO index and the simultaneous SSTA reemergence in the three action centers of the North Atlantic tripole pattern from January 2014 through April of 2015 (Fig. 8), when the EPC1 values exceeded  $+1 \text{ SD}$  (Fig. 3a). The NAO index from January to April 2014 was positive and decreased from February (1.34) to August ( $-1.68$ ). Then in September there was a sharp jump in the NAO index (1.62) and again a decrease in October ( $-1.27$ ). After that, a period of gradual increase in the NAO index began with a maximum in December (1.86). Figure 8 also shows the depth–time distribution of temperature anomalies from January 2014 to April 2015. Both winters are characterized by the SSTA tripole pattern associated with the NAO positive phase. In the HIGH and LOW (MID) regions, during February–April 2014, negative (positive) SSTAs were noted in the mixed layer. Warm SSTAs (greater than  $0.4 \text{ }^\circ\text{C}$ ) are observed off the east coast of the United States and cold SSTAs (ranging  $-0.5 \text{ }^\circ\text{C}$  to  $-0.7 \text{ }^\circ\text{C}$ ) in tropical and subpolar latitudes. These SSTAs in the HIGH and MID (LOW) regions are replaced by SSTAs of the opposite sign during the summer (autumn) of 2014. The NAO index in August and October 2014 was also negative. In the subsurface layer, temperature anomalies persist in summer, the sign of which was established in the previous winter, in the depth range of 50–500 m for the HIGH region, 50–180 m for the MID region, and 30–100 m for the LOW region. In October–November 2014, the subsurface temperature anomaly returns to the surface layer as the mixed layer deepens again.

Figure 8 also shows the climatological and actual MLD values in the regions under consideration. In the HIGH region, the change in the MLD is not noticeable. However, in other regions, the positive (negative) SSTA from January to April 2014 was accompanied by a shallower (deeper) than average MLD. In the LOW region, the negative temperature anomaly in the subsurface layer in summer was accompanied by a thinner than average MLD. The impact of the reemerging signal on the MLD in the following fall is small. This is consistent with MLD composites on Fig. 6, the patterns of correlations on Fig. 7a and composite analysis from Table 2.

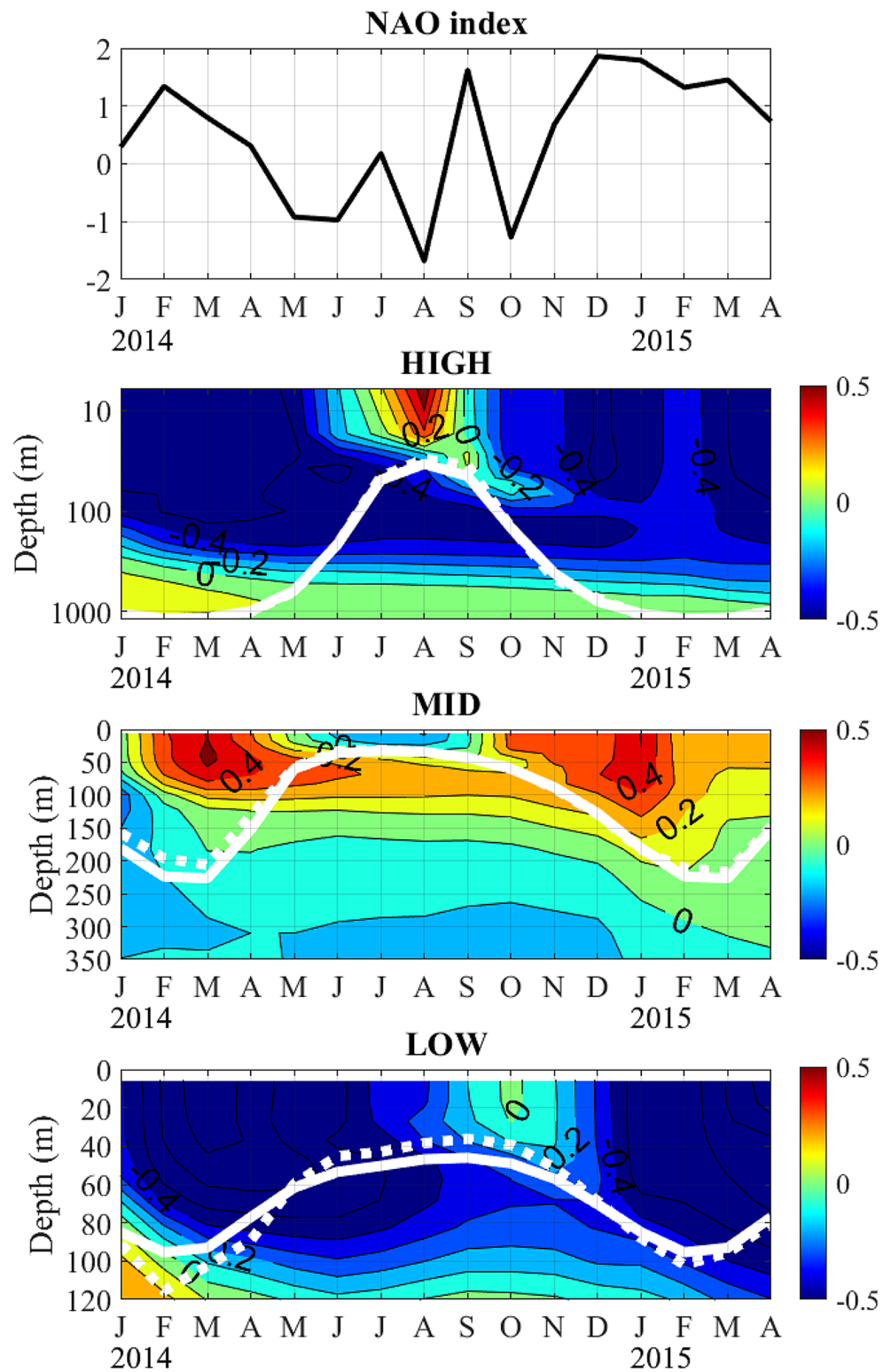
Thus, the NAO index temporal variability and the behavior of temperature anomalies at the centers of action of the tripole pattern from January 2014 to April 2015 are highly consistent. This example suggests that the reemergence of the SSTA tripole pattern formed during a certain NAO phase in the first winter may contribute to the preservation of the same NAO phase in the next winter season.

## 4 Discussion

Using EEOF for analyzing the reemergence made it possible to follow the evolution of the leading pattern of temperature anomalies over the North Atlantic in each month from January to April of the next year (Fig. 4). It was found that basin-wide reemergence occurs in the 0–300 m layer. We have also shown that about  $2/3$  of the original signal is retained in the following winter, which is consistent with the findings of Sukhonos and Alexander (2023) and is generally consistent with the EOF analysis in the time–depth plane in (Fig. 6 in Timlin et al. 2002).

All centers of action of the tripole structure in the North Atlantic show evidence of the reemergence mechanism. In the subpolar and midlatitude centers of action, the reemerging signal maximum appears in the subsurface layer in late summer and early autumn. In the subsequent autumn–winter season,  $\sim 2/3$  of this signal reaches the surface. The MID region almost coincides with the regions, examined in several studies (Hanawa and Sugimoto 2004; Timlin et al. 2002; Sukhonos and Diansky 2021). The main features of the reemergence process in this region are consistent with our results. These papers also describe the SSTA reemergence in the eastern Subpolar Atlantic. While in our paper the HIGH region, corresponding to the northern center of action of the tripole pattern, is located in the western Subpolar Atlantic. In the subtropical center of action, the maximum of the reemerging signal occurs in the mixed layer in winter–spring, and approximately one half of this signal appears at the surface in the next winter. This finding is consistent with the results of model studies (Watanabe and

**Fig. 8** (upper panel) Monthly time series of the NAO index from January 2014 to April 2015. (lower panels) Evolution of temperature anomalies (contour interval of 0.1 °C) in the three centers action of the North Atlantic tripole pattern HIGH (45°N–61°N 55°W–30°W, 0–1200 m), MID (25°N–40°N 80°W–47°W, 0–350 m) and LOW (15°N–25°N 40°W–10°W, 0–120 m) from the GECCO3 dataset from January 2014 to April 2015. The color scale in all figures is the same. The white–solid (white–dashed) lines denote climatological (actual) MLD in the considered regions. The vertical axis in the graph for the HIGH region is plotted on a logarithmic scale



Kimoto 2000; Zhao and Haine 2005; Cassou et al. 2007), and the observational analysis of de Coëtlogon and Frankignoul (2003), which are based only on SST. Zhao and Li (2010) using the lag correlation of SSTA in the region (17°–30° N 20°–50° W) found that the peak of the recurrence

is October–November (their Fig. 3). This region intersects with our LOW region, but the results of the EEOF analysis, including all levels in the 0–120 m layer, indicate that the variance maximum at the ocean surface occurs in December.

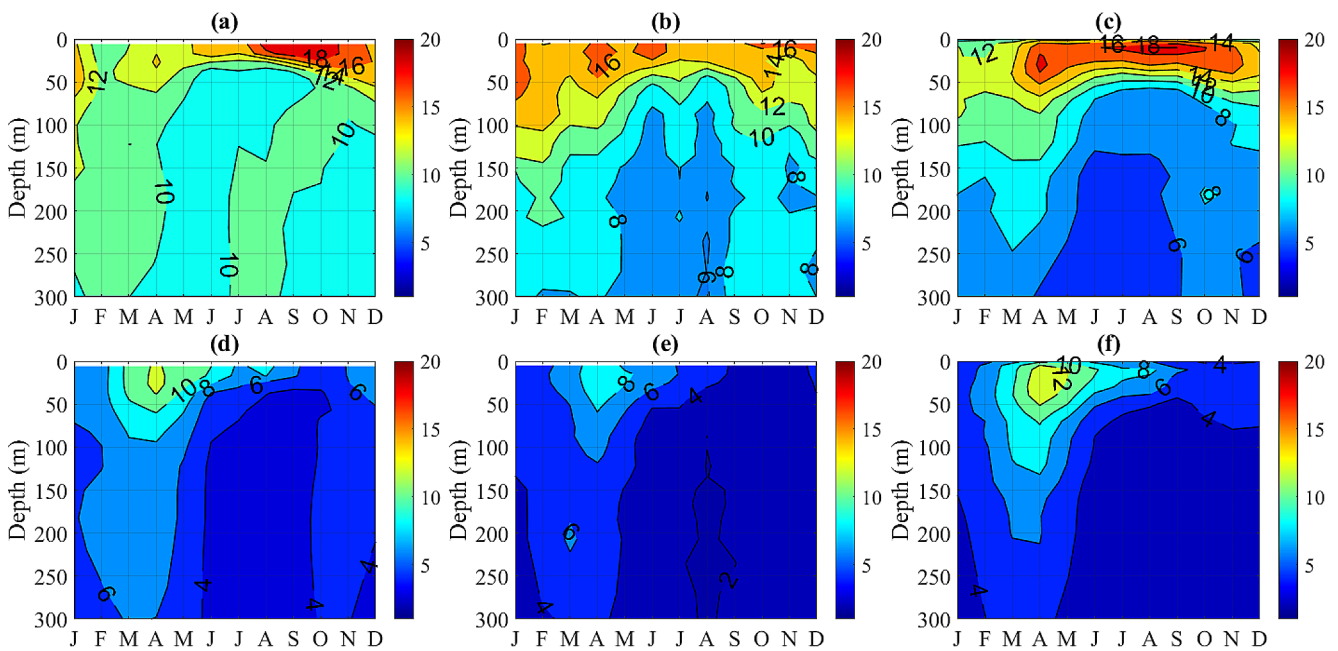


**Fig. 9** The percent variance of monthly temperature anomalies in the 0–300 m layer explained by the AMO index for the North Atlantic domain (15°N–70°N) from GECCO3 (**a**, **d**), EN4 (**b**, **e**) and IAP (**c**, **f**)

The NAO – large-scale pattern of extratropical atmospheric circulation variability is driven primarily by internal nonlinear dynamical processes (Deser et al. 2010). Much of the variability in the NAO is due to random weather noise and does not require external forcing to exist. As a result, it is possible for the winter NAO to have the same sign in two consecutive years due to random fluctuations. However, this pattern can also respond to external forcing, both natural (Stenchikov et al. 2002; Peings and Magnusdottir 2016) and anthropogenic (Ulbrich and Christoph 1999). Our results are obtained after removing low-frequency variability from the NAO index time series. If the NAO had a low-frequency component of variability (due to global warming or Atlantic Multidecadal Oscillation), then this could provide a consistent forcing from the NAO from one winter to the next. This, in turn, would result in the SSTA recurrence between winters due to the same NAO forcing in both winters rather than due to reemergence. One of the types of natural (oceanic) forcing can be the simultaneous reemergence of SSTAs formed in the previous winter in all centers of action of the tripole located in different latitudinal zones of the North Atlantic. The role of the SSTA reemergence may predominate, when other forcings are small, and when the NAO-related SSTA tripole has large amplitude, for example, as in 2010. Taws et al. (2011), Maidens et al. (2013) and Buchan et al. (2014) showed that the extremely negative NAO at the end of 2010 was partly due to the SSTA reemergence formed in the previous winter with negative NAO conditions. There was intense air–sea interaction in the eastern

Subpolar Atlantic during the winter of 2013–2014 (Grist et al. 2016), which led to the formation of significant negative SSTAs that underwent reemergence. The negative SSTA did reappear in November 2014, which is in full agreement with our results obtained for the western Subpolar Atlantic (the HIGH region). Our results also show the persistence of temperature anomalies in all centers of action of the tripole structure from January 2014 to April 2015 associated with the repeated positive NAO phase. In addition, both cases of the SSTA reemergence formed in 2010 and 2014 were accompanied by severe weather conditions on the continents adjacent to the North Atlantic (Taws et al. 2011; Grist et al. 2016; and references therein).

The NAO organizes surface fluxes (including wind stress and its curl, and buoyancy fluxes) and the ocean responds to the surface flux forcing. Results of modeling studies (Eden and Willebrand 2001; Gulev et al. 2003; Barrier et al. 2014; Khatri et al. 2022) showed that the fast ( $\leq$  two seasons) ocean response to the winter NAO forcing involves SST changes from surface heat flux anomalies and wind-induced changes in Ekman transport. The influence of the surface heat fluxes on the SSTA tripole formation in the first winter is clear in our analysis and previous studies (e.g., Cayan 1992; Deser et al. 2010). Eden and Willebrand (2001) and Gulev et al. (2003) also determined that the intensity of the ocean meridional circulation and meridional heat transport can have a rapid response to the wind stress curl. On decadal and longer time scales, the ocean dynamically adjusts to the changes in wind stress curl, which in turn, affects SST

(Marshall et al. 2001; Visbeck et al. 2003). The results, associated with wind stress curl, generally relate to longer time scales than the primary reemergence signal, which is mainly annual or perhaps out to two years. On longer than seasonal time scales, the wind stress curl is critical for driving ocean currents and subduction. Interannual and lower-frequency changes in the North Atlantic wind stress curl cause changes in large-scale ocean circulation, such as: fluctuations in the depth of the thermocline in the subtropical gyre (Sturges et al. 1998), meridional displacements of the subtropical gyre (Häkkinen and Rhines 2009), changes in the position of the North Atlantic Current axis (White and Heywood 1995), and variability of North Atlantic currents: including the Labrador (Han and Tang 2001; Spall and Pickart 2003), Florida (DiNezio et al. 2009) and Norwegian (Orvik and Skagseth 2003) currents. So it is possible that wind stress curl variability could influence the reemergence (including remote reemergence) by adjustment of currents and water masses at depth that could leave the surface layer by subduction or be brought back to the surface by the reverse process (obduction). These longer time scale phenomena may have a secondary influence on reemergence, perhaps making it stronger or weaker during different periods. We examined wind stress not only from its role in forcing the ocean in the first winter but also on the feedback to the atmosphere in the second winter, where we did find a signal. We did not find clear evidence for this feedback in the second winter in the net surface heat fluxes available from the ocean reanalyses used here.

Wang et al. (2004) analyzed the causal relation between NAO and the whole North Atlantic SST field using the Granger causality technique on seasonal time scales over the period 1948–2000. They showed that the anomalous SSTs around the Gulf Stream extension are important in initiating disturbances of the atmospheric circulation over the wintertime North Atlantic. Mosedale et al. (2006), using the Granger causality approach and daily data, found that the North Atlantic SST tripole pattern provide additional predictive information for the NAO. Much of this effect is concentrated in the region of the Gulf Stream, especially south of Cape Hatteras. Granger analysis in our study indicates that there is a small, yet statistically significant positive feedback of SSTAs, which reemerged in three centers of the tripole pattern in late autumn and early winter, on the simultaneous NAO variability. We note that Granger analysis provides a statistical assessment of feedbacks but does not consider dynamic processes associated with air–sea interaction. Despite these limitations, the Granger causality test is stricter and more reliable than simple lagged correlations (Wang et al. 2004; McGraw and Barnes 2018).

Evidence for weak positive feedback of the SSTA tripole reemergence on the NAO during the late fall and early winter

was also obtained in a number works (e.g., Watanabe and Kimoto 2000; Czaja and Frankignoul 2002; Cassou et al. 2007; Gastineau and Frankignoul 2015; Grist et al. 2019). Note that the SSTA tripole pattern reemergence is a process that covers the upper layer of the ocean over a wide area. While many factors, including stochastic variability, can cause a change in the NAO, SSTA reemergence of the same sign as in the previous winter, defined by EPC1 time series, could act to maintain the NAO phase. The reemergence of a large-scale tripole structure of temperature anomalies in the North Atlantic may be one of the processes determining the thermal inertia of the upper ocean layer, which enhances NAO variability on interannual to decadal scales.

## 5 Conclusions

We utilized GECCO3, ORA-S5 and SODA3.12.2 reanalyses to examine the SSTA tripole pattern reemergence in the North Atlantic, with a particular focus on the analysis of the features of the SSTA reemergence in the SSTA tripole centers of action and the association with the NAO. The results are based on decomposition of ocean reanalyses data using extended EOFs and the Granger causality technique.

The leading pattern during the entire 16-month period (January–April of the following year) in the North Atlantic 0–300 m layer is a tripole with temperature anomalies of the same sign in the tropical and subpolar latitudes and the opposite sign in the subtropical gyre. The evolution of the leading pattern for the entire basin (EPC1) shows the deepening of temperature anomalies in winter, their persistence with a maximum in the summer seasonal thermocline (~65–90 m in August–September) and partial weakening in the subsurface layer in summer, and their emergence on the ocean surface in the subsequent autumn–winter. On the ocean surface, the tripole pattern is well manifested in the first and subsequent winters, but is poorly detected in summer. In the subsurface layer, the tripole structure persists throughout the entire 16-month period. The regions with high correlations in absolute value between the EPC1 with the time series of monthly temperature anomalies at individual grid points in the subsurface layer is largest in March (when the MLD is at its maximum) and gradually decreases towards April of the following year. Areas of high correlations in absolute value on the ocean surface in the following winter (from November to March of the following year) emerge above the areas of high correlations in absolute value in the subsurface layer, forming a tripole structure.

The temporal evolution of the SSTA tripole reemergence in the North Atlantic domain, explained by the EPC1, is in good agreement with the variability of the main atmospheric circulation mode over the North Atlantic on the

interannual scales – the NAO, especially after 1979. Based on Granger analysis a unidirectional relationship between the NAO in January–March and EPC1 was revealed with high reliability (at a confidence level of 97.5%). Accounting for the NAO variability in the first winter makes it possible to reduce the error in predicting the EPC1 values by almost a quarter. A bidirectional relationship was found between NAO in November (in GECCO3 data) and December (in ORAS5 and SODA3 datasets) and EPC1 with moderate confidence (90% level). Accounting for additional information about EPC1 (NAO) in late autumn and early winter in the NAO (EPC1) joint model makes it possible to reduce the prediction error by one sixth. Thus, the temperature anomalies formed in January–March under the NAO forcing in the centers of action of tripole pattern and reemerged from the subsurface layer in November–December will contribute to a change in the large-scale atmospheric circulation towards the NAO phase that formed these anomalies.

The behavior of temperature anomalies involved in the reemergence process is fully consistent with the upper mixed layer dynamics for the chosen criterion for determining the position of the upper mixed layer lower boundary. The reemergence of temperature anomalies is accompanied by a change in vertical stratification. The reemergence of a negative (positive) temperature anomaly leads to the MLD deepening (shallowing) in the first winter and MLD shallowing (deepening) in the summer.

## Appendix

### Robustness of removing of multidecadal variability

Let us consider how effective removing a 3rd degree polynomial from ocean temperature time series suppresses the signal of multidecadal variability. For this purpose, monthly mean values of the North Atlantic ocean (15°–70° N) temperature from the GECCO3 reanalysis (as in the paper) and objective analysis datasets of EN.4.2.2 (Good et al. 2013) and IAP (Cheng and Zhu 2016) were used. Two additional data sets were also analyzed to increase the reliability of the conclusions drawn from the GECCO3 data. There are 20 levels in the 0–300 m layer in EN4 data and 19 levels in IAP data. Monthly averages of the Atlantic Multidecadal Oscillation (AMO) index were taken from the website (<https://climatedataguide.ucar.edu/climate-data/atlantic-multi-decadal-oscillation-amo>). All these datasets cover the period from 1948 to 2018. Next, the percent variance of monthly temperature anomalies explained by the AMO

index is calculated using Eq. (1). However, in this calculation,  $r$  is the correlation coefficient between the time series of temperature anomalies and the AMO index,  $\sigma$  is the standard deviation of the temperature anomalies,  $i$  indicates an individual grid point, and  $N$  is the total number of grid points.

The results are shown in Fig. 9. In the first case (upper panels), to show the net contribution of multidecadal variability, the linear trend for the period 1948–2018 was removed from the ocean temperature data used, the coefficients of which were calculated using the least squares method. The high AMO contribution (> 12%) is located on average in the upper 100 m layer. With increasing depth this contribution decreases. Moreover, in the winter months the thickness of the layer with a high contribution of AMO is greater, and in the summer months the thickness of this layer is less, which corresponds to the seasonal cycle of the upper mixed layer. The greatest contribution of AMO (> 18%) is observed in the surface layer from August to October. Overall variance explained by the AMO index averaged over all months of the year in the 0–300 m layer after removing linear trend is ~11.4% for GECCO3, ~7.4% for EN4 and ~10.4% for IAP of the total variance.

In the second case (bottom panels), a third-degree polynomial for the period 1948–2018 was removed from the ocean temperature data used, the coefficients of which were calculated using the least squares method. Overall variance explained by the AMO index averaged over all months of the year in the 0–300 m layer after 3rd order polynomial removing decreases by a factor of 2. The percent variance of temperature anomalies in the upper 300 m layer explained by the AMO index is less than 8%. The exception is the upper 50 m layer in April (~10–12%).

Thus, the procedure of removing a 3rd degree polynomial from ocean temperature time series allows, if not completely filtering out multidecadal variability, then effectively reducing the amplitude of the signal at this time scale. Note that removing a first degree polynomial is usually used to analyze the underlying modes of natural climate variability. This suggests that forced climate evolution is essentially linear in time, although observations and climate modeling suggest otherwise. Analysis of large ensembles has shown that linear trend removing is ineffective for separating anthropogenic and other external forcing from SST changes (Frankignoul et al. 2017).

**Acknowledgements** The authors thank the anonymous reviewers for the constructive and insightful comments, which have helped us to improve our manuscript. The authors would like to thank internal reviewer for helpful suggestions. The authors are grateful to the editorial team for professional editing of the work.

**Author contributions** P.S. conceived the study, performed the analysis and wrote the first draft of the manuscript. All authors contributed to



the design of the study, interpretation and presentation of results, and writing and revision of the manuscript. All authors read and approved the final manuscript.

**Funding** The work of P.S. was supported by Russian Science Foundation (project No. 23–77–01054).

**Data availability** All data used in this study are available from publicly accessible data archives.

## Declarations

**Conflict of interest** The authors declare no conflict of interest.

## References

- Alexander MA, Deser C (1995) A mechanism for the recurrence of wintertime midlatitude SST anomalies. *J Phys Oceanogr* 25(1):122–137. [https://doi.org/10.1175/1520-0485\(1995\)025%3c0122:AMFTRO%3e2.0.CO;2](https://doi.org/10.1175/1520-0485(1995)025%3c0122:AMFTRO%3e2.0.CO;2)
- Alexander MA, Deser C, Timlin MS (1999) The reemergence of SST anomalies in the North Pacific Ocean. *J Clim* 12(8):2419–2433. [https://doi.org/10.1175/1520-0442\(1999\)012%3C2419:TROSAI%3E2.0.CO;2](https://doi.org/10.1175/1520-0442(1999)012%3C2419:TROSAI%3E2.0.CO;2)
- Alexander MA, Scott JD, Deser C (2000) Processes that influence sea surface temperature and ocean mixed layer depth variability in a coupled model. *J Geophys Res: Oceans* 105(C7):16823–16842. <https://doi.org/10.1029/2000JC900074>
- Alexander MA, Timlin MS, Scott JD (2001) Winter-to-winter recurrence of sea surface temperature, salinity and mixed layer depth anomalies. *Prog Oceanogr* 49(1–4):41–61. [https://doi.org/10.1016/S0079-6611\(01\)00015-5](https://doi.org/10.1016/S0079-6611(01)00015-5)
- Barrier N, Cassou C, Deshayes J, Treguier A-M (2014) Response of North Atlantic ocean circulation to atmospheric weather regimes. *J Phys Oceanogr* 44(1):179–201. <https://doi.org/10.1175/JPO-D-12-0217.1>
- Box GEP, Jenkins GM (1976) *Time Series Analysis: Forecasting and Control*. San Francisco, CA: Holden-Day. 575 p
- Buchan J, Hirschi JJ, Blaker AT, Sinha B (2014) North Atlantic SST anomalies and the cold north European weather events of winter 2009/10 and December 2010. *Mon Weather Rev* 142(2):922–932. <https://doi.org/10.1175/MWR-D-13-00104.1>
- Byju P, Dommengot D, Alexander MA (2018) Widespread reemergence of sea surface temperature anomalies in the global oceans, including tropical regions forced by reemerging winds. *Geophys Res Lett* 45(15):7683–7691. <https://doi.org/10.1029/2018GL079137>
- Carton JA, Chepurin GA, Chen L (2018) SODA3: a new ocean climate reanalysis. *J Clim* 31(17):6967–6983. <https://doi.org/10.1175/JCLI-D-18-0149.1>
- Cassou C, Deser C, Alexander MA (2007) Investigating the impact of reemerging sea surface temperature anomalies on the winter atmospheric circulation over the North Atlantic. *J Clim* 20(14):3510–3526. <https://doi.org/10.1175/JCLI4202.1>
- Cayan DR (1992) Latent and sensible heat flux anomalies over the northern oceans: driving the sea surface temperature. *J Phys Oceanogr* 22(8):859–881. [https://doi.org/10.1175/1520-0485\(1992\)022%3C0859:LASHFA%3E2.0.CO;2](https://doi.org/10.1175/1520-0485(1992)022%3C0859:LASHFA%3E2.0.CO;2)
- Cheng L, Zhu J (2016) Benefits of CMIP5 multimodel ensemble in reconstructing historical ocean subsurface temperature variation. *J Clim* 29(15):5393–5416. <https://doi.org/10.1175/JCLI-D-15-0730.1>
- Czaja A, Frankignoul C (2002) Observed impact of Atlantic SST anomalies on the North Atlantic Oscillation. *J Clim* 15(6):606–623. [https://doi.org/10.1175/1520-0442\(2002\)015%3C0606:OIOASA%3E2.0.CO;2](https://doi.org/10.1175/1520-0442(2002)015%3C0606:OIOASA%3E2.0.CO;2)
- de Coëtlogon G, Frankignoul C (2003) The persistence of winter sea surface temperature in the North Atlantic. *J Clim* 16(9):1364–1377. [https://doi.org/10.1175/1520-0442\(2003\)16%3e1364:TPOWSS%3e2.0.CO;2](https://doi.org/10.1175/1520-0442(2003)16%3e1364:TPOWSS%3e2.0.CO;2)
- Deser C, Alexander MA, Timlin MS (2003) Understanding the persistence of sea surface temperature anomalies in midlatitudes. *J Clim* 16(1):57–72. [https://doi.org/10.1175/1520-0442\(2003\)016%3C0057:UTPOSS%3E2.0.CO;2](https://doi.org/10.1175/1520-0442(2003)016%3C0057:UTPOSS%3E2.0.CO;2)
- Deser C, Alexander MA, Xie S-P, Phillips AS (2010) Sea surface temperature variability: patterns and mechanisms. *Annu Rev Mar Sci* 2:115–143. <https://doi.org/10.1146/annurev-marine-120408-151453>
- DiNezio PN, Gramer LJ, Johns WE, Meinen CS, Baringer MO (2009) Observed interannual variability of the Florida Current: wind forcing and the North Atlantic Oscillation. *J Phys Oceanogr* 39(3):721–736. <https://doi.org/10.1175/2008JPO4001.1>
- Eden C, Willebrand J (2001) Mechanism of interannual to decadal variability of the North Atlantic circulation. *J Clim* 14(10):2266–2280. [https://doi.org/10.1175/1520-0442\(2001\)014%3C2266:MOITDV%3E2.0.CO;2](https://doi.org/10.1175/1520-0442(2001)014%3C2266:MOITDV%3E2.0.CO;2)
- Elsner JB (2007) Granger causality and Atlantic hurricanes. *Tellus* 59(4):476–485. <https://doi.org/10.1111/j.1600-0870.2007.00244.x>
- Frankignoul C, Gastineau G, Kwon Y-O (2017) Estimation of the SST response to anthropogenic and external forcing and its impact on the Atlantic multidecadal oscillation and the Pacific decadal oscillation. *J Clim* 30(24):9871–9895. <https://doi.org/10.1175/JCLI-D-17-0009.1>
- Frankignoul C, Kestenare E, Reverdin G (2021) Sea surface salinity reemergence in an updated North Atlantic in situ salinity dataset. *J Clim* 34(22):9007–9023. <https://doi.org/10.1175/JCLI-D-20-0840.1>
- Gastineau G, Frankignoul C (2015) Influence of the North Atlantic SST variability on the atmospheric circulation during the twentieth century. *J Clim* 28(4):1396–1416. <https://doi.org/10.1175/JCLI-D-14-00424.1>
- Good SA, Martin MJ, Rayner NA (2013) EN4: quality controlled ocean temperature and salinity profiles and monthly objective analyses with uncertainty estimates. *J Geophys Res: Oceans* 118(12):6704–6716. <https://doi.org/10.1002/2013JC009067>
- Granger CWJ (1969) Investigating causal relations by econometric models and cross-spectral methods. *Econometrica* 37(3):424–438. <https://doi.org/10.2307/1912791>
- Grist JP, Josey SA, Jacobs ZL, Marsh R, Sinha B, Seville EV (2016) Extreme air–sea interaction over the North Atlantic subpolar gyre during the winter of 2013–2014 and its sub-surface legacy. *Clim Dyn* 46:4027–4045. <https://doi.org/10.1007/s00382-015-2819-3>
- Grist JP, Sinha B, Hewitt HT, Duchez A, MacLachlan C, Hyder P, Josey SA, Hirschi JJ-M, Blaker AT, New AL, Scaife AA, Roberts CD (2019) Re-emergence of North Atlantic subsurface ocean temperature anomalies in a seasonal forecast system. *Clim Dyn* 53(7):4799–4820. <https://doi.org/10.1007/s00382-019-04826-w>
- Gulev SK, Barnier B, Knochel H, Molines J-M, Cottet M (2003) Water mass transformation in the North Atlantic and its impact on the meridional circulation: insights from an ocean model forced by NCEP–NCAR reanalysis surface fluxes. *J Clim* 16(19):3085–3110. [https://doi.org/10.1175/1520-0442\(2003\)016%3C3085:WMTITN%3E2.0.CO;2](https://doi.org/10.1175/1520-0442(2003)016%3C3085:WMTITN%3E2.0.CO;2)
- Häkkinen S, Rhines PB (2009) Shifting surface currents in the northern North Atlantic Ocean. *J Geophys Res* 114(C4):C04005. <https://doi.org/10.1029/2008JC004883>

- Han G, Tang CL (2001) Interannual variations of volume transport in the western Labrador Sea based on TOPEX/Poseidon and WOCE data. *J Phys Oceanogr* 31(1):199–211. [https://doi.org/10.1175/1520-0485\(2001\)031%3C0199:IVOVTI%3E2.0.CO;2](https://doi.org/10.1175/1520-0485(2001)031%3C0199:IVOVTI%3E2.0.CO;2)
- Hanawa K, Sugimoto S (2004) «Reemergence» areas of winter sea surface temperature anomalies in the world's oceans. *Geophys Res Lett* 31(10):L10303. <https://doi.org/10.1029/2004GL019904>
- Hannachi A (2004) A primer for EOF analysis of climate data. Department of Meteorology, University of Reading, Reading, UK, p 33
- Junge MM, Haine TWN (2001) Mechanisms of North Atlantic wintertime sea surface temperature anomalies. *J Clim* 14(24):4560–4572. [https://doi.org/10.1175/1520-0442\(2001\)014%3C4560:M ONAWS%3E2.0.CO;2](https://doi.org/10.1175/1520-0442(2001)014%3C4560:M ONAWS%3E2.0.CO;2)
- Khatri H, Williams RG, Woollings T, Smith DM (2022) Fast and slow subpolar ocean responses to the North Atlantic Oscillation: thermal and dynamical changes. *Geophys Res Lett* 49(24). <https://doi.org/10.1029/2022GL101480>. e2022GL101480
- Köhl A (2020) Evaluating the GECCO3 1948–2018 ocean synthesis—a configuration for initializing the MPI-ESM climate model. *Q J R Meteorol Soc* 146(730):2250–2273. <https://doi.org/10.1002/qj.3790>
- Lau NC, Philander SGH, Nath MJ (1992) Simulation of ENSO-like phenomena with a low-resolution coupled GCM of the global ocean and atmosphere. *J Clim* 5(4):284–307. [https://doi.org/10.1175/1520-0442\(1992\)005%3C0284:SOELPW%3E2.0.CO;2](https://doi.org/10.1175/1520-0442(1992)005%3C0284:SOELPW%3E2.0.CO;2)
- Maidens A, Arribas A, Scaife AA, MacLachlan C, Peterson D, Knight J (2013) The influence of surface forcings on prediction of the North Atlantic oscillation regime of winter 2010/11. *Mon Weather Rev* 141(11):3801–3813. <https://doi.org/10.1175/MWR-D-13-00033.1>
- Marshall J, Schott F (1999) Open-ocean convection: observations, theory, and models. *Rev Geophys* 37(1):1–64. <https://doi.org/10.1029/98RG02739>
- Marshall J, Johnson H, Goodman J (2001) A study of the interaction of the North Atlantic Oscillation with ocean circulation. *J Clim* 14(7):1399–1421. [https://doi.org/10.1175/1520-0442\(2001\)014%3C1399:ASOTIO%3E2.0.CO;2](https://doi.org/10.1175/1520-0442(2001)014%3C1399:ASOTIO%3E2.0.CO;2)
- McGraw MC, Barnes EA (2018) Memory matters: a case for Granger causality in climate variability studies. *J Clim* 31(8):3289–3300. <https://doi.org/10.1175/JCLI-D-17-0334.1>
- Mokhov II, Smirnov DA, Nakonechny PI, Kozlenko SS, Seleznev EP, Kurths J (2011) Alternating mutual influence of El-Niño/Southern Oscillation and Indian monsoon. *Geophys Res Lett* 38(8):L00F04. <https://doi.org/10.1029/2010GL045932>
- Monterey GI, Levitus S (1997) Seasonal variability of mixed layer depths for the World. NOAA Atlas NESDIS 14, 100 pp., Natl. Oceanic and Atmos. Admin., Silver Spring, Md. [https://repository.noaa.gov/view/noaa/49153/noaa\\_49153\\_DS1.pdf](https://repository.noaa.gov/view/noaa/49153/noaa_49153_DS1.pdf)
- Mosedale TJ, Stephenson DB, Collins M, Mills TC (2006) Granger causality of coupled climate processes: Ocean feedback on the North Atlantic Oscillation. *J Clim* 19(7):1182–1194. <https://doi.org/10.1175/JCLI3653.1>
- Namias J, Born RM (1970) Temporal coherence in North Pacific sea-surface temperature patterns. *J Geophys Res* 75(30):5952–5955. <https://doi.org/10.1029/JC075i030p05952>
- Orvik KA, Skagseth O (2003) The impact of the wind stress curl in the North Atlantic on the Atlantic inflow to the Norwegian Sea toward the Arctic. *Geophys Res Lett* 30(17):1884. <https://doi.org/10.1029/2003GL017932>
- Peings Y, Magnusdottir G (2016) Wintertime atmospheric response to Atlantic multidecadal variability: effect of stratospheric representation and ocean–atmosphere coupling. *Clim Dyn* 47(3–4):1029–1047. <https://doi.org/10.1007/s00382-015-2887-4>
- Schwarz G (1978) Estimating the dimension of a model. *Annals Stat* 6(2):461–464. <https://www.jstor.org/stable/2958889>
- Seber GA, Lee AJ (2012) Linear Regression Analysis. John Wiley & Sons: Hoboken, NJ, USA. V. 329
- Shapiro SS, Wilk MB (1965) An analysis of variance test for normality: complete samples. *Biometrika* 52(3):591–611. <https://doi.org/10.2307/2333709>
- Spall MA, Pickart RS (2003) Wind-driven recirculations and exchanges in the Labrador and Irminger seas. *J Phys Oceanogr* 33(8):1829–1845. [https://doi.org/10.1175/1520-0485\(2003\)033%3C1829:WRAEIT%3E2.0.CO;2](https://doi.org/10.1175/1520-0485(2003)033%3C1829:WRAEIT%3E2.0.CO;2)
- Stenchikov G, Robock A, Ramaswamy V, Schwarzkopf MD, Hamilton K, Ramachandran S (2002) Arctic Oscillation response to the 1991 Mount Pinatubo eruption: effects of volcanic aerosols and ozone depletion. *J Geophys Res* 107(D24):4803. <https://doi.org/10.1029/2002JD002090>
- Strong C, Magnusdottir G, Stern H (2009) Observed feedback between winter sea ice and the North Atlantic Oscillation. *J Clim* 22(22):6021–6032. <https://doi.org/10.1175/2009JCLI3100.1>
- Sturges W, Hong BG, Clarke AJ (1998) Decadal wind forcing of the North Atlantic subtropical gyre. *J Phys Oceanogr* 28(4):659–668. [https://doi.org/10.1175/1520-0485\(1998\)028%3C0659:DWFOTN%3E2.0.CO;2](https://doi.org/10.1175/1520-0485(1998)028%3C0659:DWFOTN%3E2.0.CO;2)
- Sugimoto S, Hanawa K (2005) Why does reemergence of winter sea surface temperature anomalies not occur in eastern mode water areas? *Geophys Res Lett* 32(15):L15608. <https://doi.org/10.1029/2005GL022968>
- Sukhonos PA, Alexander MA (2023) The reemergence of the winter sea surface temperature tripole in the North Atlantic from ocean reanalysis data. *Clim Dyn* 61(1–2):449–460. <https://doi.org/10.1007/s00382-022-06581-x>
- Sukhonos PA, Diansky NA (2021) Analysis of the reemergence of winter anomalies of upper ocean characteristics in the North Atlantic from reanalysis data. *Izv Atmos Ocean Phys* 57(3):310–320. <https://doi.org/10.1134/S0001433821030099>
- Taws SL, Marsh R, Wells NC, Hirschi J (2011) Re-emerging ocean temperature anomalies in late-2010 associated with a repeat negative NAO. *Geophys Res Lett* 38(20):L20601. <https://doi.org/10.1029/2011GL048978>
- Timlin MS, Alexander MA, Deser C (2002) On the reemergence of North Atlantic SST anomalies. *J Clim* 15(18):2707–2712. [https://doi.org/10.1175/1520-0442\(2002\)015%3c2707:OTRONA%3e2.0.CO;2](https://doi.org/10.1175/1520-0442(2002)015%3c2707:OTRONA%3e2.0.CO;2)
- Ulbrich U, Christoph M (1999) A shift of the NAO and increasing storm track activity over Europe due to anthropogenic greenhouse gas forcing. *Clim Dyn* 15:551–559. <https://doi.org/10.1007/s003820050299>
- Visbeck M, Chassignet EP, Curry RG, Delworth TL, Dickson RR, Krahnemann G (2003) The ocean's response to North Atlantic Oscillation variability. *North Atl Oscillation: Clim Significance Environ Impact* 134:113–145
- Wang W, Anderson BT, Kaufmann RK, Myneni RB (2004) The relation between the North Atlantic Oscillation and SSTs in the North Atlantic basin. *J Clim* 17(24):4752–4759. <https://doi.org/10.1175/JCLI-3186.1>
- Watanabe M, Kimoto M (2000) On the persistence of decadal SST anomalies in the North Atlantic. *J Clim* 13(16):3017–3028. [https://doi.org/10.1175/1520-0442\(2000\)013%3c3017:OTPODS%3e2.0.CO;2](https://doi.org/10.1175/1520-0442(2000)013%3c3017:OTPODS%3e2.0.CO;2)
- Weare BC, Nasstrom JS (1982) Examples of extended empirical orthogonal function analyses. *Mon Wea Rev* 110(6):481–485. [https://doi.org/10.1175/1520-0493\(1982\)110%3C0481:EOEEOF%3E2.0.CO;2](https://doi.org/10.1175/1520-0493(1982)110%3C0481:EOEEOF%3E2.0.CO;2)
- White MA, Heywood KJ (1995) Seasonal and interannual changes in the North Atlantic subpolar gyre from Geosat and TOPEX/

- POSEIDON altimetry. *J Geophys Res* 100(C12):24931–24941. <https://doi.org/10.1029/95JC02123>
- Zhao B, Haine TWN (2005) On processes controlling seasonal North Atlantic sea surface temperature anomalies in ocean models. *Ocean Model* 9(3):211–229. <https://doi.org/10.1016/j.ocemod.2004.05.001>
- Zhao X, Li J (2010) Winter-to-winter recurrence of sea surface temperature anomalies in the Northern Hemisphere. *J Clim* 23(14):3835–3854. <https://doi.org/10.1175/2009JCLI2583.1>
- Zuo H, Balmaseda MA, Tietsche S, Mogensen K, Mayer M (2019) The ECMWF operational ensemble reanalysis–analysis system for ocean and sea ice: a description of the system and assessment. *Ocean Sci* 15(3):779–808. <https://doi.org/10.5194/os-15-779-2019>

**Publisher's Note** Springer Nature remains neutral with regard to jurisdictional claims in published maps and institutional affiliations.

Springer Nature or its licensor (e.g. a society or other partner) holds exclusive rights to this article under a publishing agreement with the author(s) or other rightsholder(s); author self-archiving of the accepted manuscript version of this article is solely governed by the terms of such publishing agreement and applicable law.